

## A novel model for glaze ice accretion

Róbert-Zoltán Szász<sup>1\*</sup>, Stefan Ivanell<sup>2</sup>, Johan Revstedt<sup>1</sup>

<sup>1</sup> Lund University, Dept. Energy Sciences, PO.Box 118, 22100 Lund, Sweden

<sup>2</sup> Uppsala University, Department of Earth Sciences, Cramergatan 3, 62167 Visby, Sweden

**Abstract:** This paper introduces a novel model to predict ice accretion in glaze ice conditions due to supercooled water droplets. Glaze icing is controlled by a large number of interacting physical phenomena. The purpose of the suggested model was to offer a faster alternative to explicitly modelling these phenomena. The paper presents the suggested model and investigates the sensitivity of the predictions on the model parameters for three experimental cases in the literature. The results indicate a qualitatively correct behavior. Quantitatively, the model over-predicts the amount of accreted ice, the error being significantly larger in severe icing conditions. The errors are caused partly by the choice of faster numerical approaches and by the lack of possibility to account for detaching ice from the surface.

**Keywords:** CFD, glaze ice, ice accretion, LPT

### 1 Introduction

Wind power technology, as one of the tools to replace fossil fuels, gained a strong popularity during the past decades. Due to the rapid increase of the number and size of installed power plants, there are more and more wind turbines installed in less favorable areas, such as areas with cold climate conditions. It is estimated that about a quarter of the global installed wind energy capacity is located in areas prone to the risk of icing (Stoyanov and Nixon (2020)). In some countries, the share of wind turbines located in cold climate areas is significantly higher, e.g. in Sweden more than 80% of the installed capacity in 2020 was located in the most northerly quarter of the country (Badman and Tengblad (2021)).

Although cold climate areas have the advantage of a generally lower population density (leading to better acceptance) and larger amount of extractable kinetic energy (for the same wind speed, due to the higher density), ice accretion imposes significant challenges for the manufacturers and for the wind turbine owners. The ice layer changes the aerodynamic shape of the blade, resulting in non-optimal profiles and a decrease of the extracted energy. Furthermore, the extra mass of the ice represents an extra load on the solid structures and may imbalance the rotor causing vibrations which lead to earlier fatigue and, in extreme cases, mechanical failures. There is a safety hazard as well, ice chunks may detach from the blades and may travel relatively large distances. These chunks represent a danger for the persons or objects located in the turbines' neighborhood. The current trend of increasing wind turbine sizes increases also the areas affected by ice throw.

The above-described challenges triggered research campaigns focusing on many aspects of ice accretion, like predicting weather conditions leading to ice accretion, investigating the accretion process itself, development of ice detection and de-icing devices, just to name a few research areas. A rather detailed overview of the related research is presented in Laakso et al. (2010).

The characteristics of the accreted ice depend on the prevailing meteorological conditions. Commonly, icing conditions are divided in two categories. In low temperature (usually below  $-10^{\circ}\text{C}$ ) conditions, the water droplets are well below freezing temperature but are still in the liquid state. These supercooled droplets impacting on a surface freeze instantaneously upon contact, and begin to accrete forming rime ice, which is usually opaque due to the air trapped between the frozen droplets. For slightly higher temperatures, but still below freezing, (usually between  $-5$  and  $0^{\circ}\text{C}$ ) the supercooled droplets do not freeze instantaneously upon contacting the surface. Instead, a water film is formed which may run along the surfaces before freezing, leading to the formation of a more compact, so-called glaze-ice. Of course, in practical situations a combination of rime and glaze conditions might occur as well.

The first studies of the impact of icing on airfoils date back to 1930's and originated in the aerospace community (Jones and Williams (1936); Gulick (1938)). Over the past two decades various authors presented more specific studies on the accretion on wind turbine blades. Makkonen (1985, 2000) was among the first ones to characterize different kind of icing events and to create models for it. Based on thermodynamic considerations the following model was proposed to predict the rate of ice accretion:

$$\frac{dM}{dt} = c_1 c_2 c_3 \phi \mathbf{u} A \quad (1)$$

where  $M$  is the mass of the ice,  $t$  the time,  $\phi$  the mass concentration of particles,  $\mathbf{u}$  the velocity of the particles relative to the object,  $A$  the cross sectional area of the object.  $c_1$ ,  $c_2$  and  $c_3$  are correction factors having values between zero and one and account for

\* E-mail address: [robert-zoltan.szasz@energy.lth.se](mailto:robert-zoltan.szasz@energy.lth.se)

doi: [10.24352/UB.OVGU-2023-054](https://doi.org/10.24352/UB.OVGU-2023-054)

2023 | All rights reserved.

the collision efficiency, sticking efficiency and accretion efficiency, respectively. For further details about the model the reader is referred e.g. to [Makkonen \(2000\)](#). Eq. 1 is still the most widely used ice prediction model, often combined with other methods. Usually, there is a scale separation between the flow field surrounding the blades and the rate of ice accretion on the blades. As a consequence, a common approach is to compute the ice accretion and the flow around the ice accreted airfoils in separate stages. For the flow computations a common approach is to use simplified methods to reduce the computational efforts. For example, a potential flow solver is used in LEWICE, although there is a possibility to import flow fields from other solvers ([Wright \(2008\)](#)), whereas the panel method is used in TURBICE (see e.g. [Homola et al. \(2010\)](#)). Another popular tool for ice predictions is GlennICE, the differences and similarities between LEWICE and GlennICE being discussed e.g. by [Wright et al. \(2008\)](#). Recently, thanks to the increase in computational power and to the need to account for 3D effects, it is more and more common to solve the full set of Navier-Stokes equations (see e.g. [Gori et al. \(2015\)](#); [Jin and Virk \(2019\)](#); [Prince Raj et al. \(2020\)](#)). Droplet transport is commonly modelled either in an Eulerian (e.g. [Prince Raj et al. \(2020\)](#)) or Lagrangian (e.g. [Szász and Fuchs \(2012\)](#); [Szász et al. \(2016\)](#); [Gori et al. \(2015\)](#)) framework. For a recent overview of existing numerical tools for ice accretion predictions the reader is referred to ([Laurendeau et al. \(2022\)](#)) and the references therein.

In the case of rime ice conditions, since all droplets hitting the surface freeze instantaneously, there is no need for heat transfer computations. The amount of droplets hitting the surface is determined explicitly or specified via the collection efficiency, depending if a lagrangian or eulerian model is used for droplet transport.

In contrast to rime ice conditions, glaze ice conditions are significantly more difficult to model due to the multitude of interacting physical phenomena. The supercooled droplets cannot be assumed any more to freeze instantaneously upon impact. The collision of droplets with wet surfaces is rather complex even in isothermal conditions. [Roisman and Tropea \(2002\)](#) discuss for example the evolution of the crown which forms in the case of high impact velocities. The impact of supercooled droplets is studied among others by [Schremb et al. \(2018\)](#) who concluded that the freezing process differs significantly whether the droplets impact on a dry surface or on ice. In the first case the nucleation is more stochastic whereas upon impact on ice, the solidification starts simultaneously with the impact. The sensitivity of ice accretion on the surface properties can be beneficial, [Antonini et al. \(2011\)](#) discuss for example the possibility to use superhydrophobic surface coatings to reduce the amount of accreted ice.

A significant part of the literature focuses on ice accretion in Super-cooled Large Droplet (SLD) conditions. Although meteorological conditions leading to the formation of such droplets are relatively seldom, the consequences of such icing events are significant. Among others, [Broeren et al. \(2005\)](#) investigated experimentally ice accretion in SLD conditions. Three categories of features were identified: horns, nodules and clear ice. The most detrimental cases from an aerodynamic point of view were found to be the cases leading to horn ice formation.

Glaze or mixed ice might be formed also in conditions normally leading to rime ice formation if ice crystals hit warmer surfaces. In such cases the melting of the impacting ice crystals has to be considered as well. [Kintea et al. \(2016\)](#) investigated such conditions and proposed a modeling approach for the relevant transport processes.

According to [Gori et al. \(2015\)](#), the most common approach to model glaze ice is to compute 1D heat transfer problems based on the so-called Stefan's problem formulated for aeronautical applications by [Messinger \(1953\)](#) and further improved by [Myers \(2001\)](#). In [Son and Kim \(2020\)](#) beside the heat transfer consideration, the evolution of the water film formed on the blade surface is accounted as well.

The modeling of supercooled water freezing imposes further challenges, since the growth process of the ice seeds in supercooled water is related to the propagation of an unstable freezing surface. More details about this issue and models for the front propagation based on the Volume of Fluid (VOF) and Level-Set methods are discussed for example by [Rauschenberger et al. \(2013\)](#). As it is described by [Vargas et al. \(2007\)](#), the nonlinear development of the ice surface instability can lead the formation of ice feathers even in glaze ice conditions.

Thus, one can conclude that there are many accurate and detailed models in the literature to predict many aspects of glaze ice accretion. Nevertheless, for large scale applications, or when the available computing resources are limited, the application of the available models would be exhaustive.

Here, we propose an alternative approach to model glaze ice formation. Instead of accounting for all the interacting physical phenomena occurring during glaze ice formation (wall film formation, its evolution along the surface, heat transfer, etc.) we propose an extension of an already existing rime ice model.

Although its grounding in physics is limited, the suggested lower order model has the advantage of significantly lower complexity, leading to faster computing times. Beside presenting the model, the goal of the paper is to investigate the performance of the suggested model to predict light and severe glaze ice conditions.

## 2 Methods

The aim of this work has been to provide a modelling approach which had to be integrated in a model chain where a large number of ice accretion cases had to be computed. For this reason the methods chosen herein are characterized by relatively high computational performance at the expense of somewhat limited accuracy.

The scale separation of the flow time scales and the time scales associated to the growth of the ice layer facilitates the use of staged computations: one determines the flow around the airfoil and then the amount of accreted ice. Nevertheless, in the case of severe icing conditions the ice structures formed on the surfaces may significantly change the flow topology. In order to account for such changes, a common approach is to divide the time interval of the entire icing event in sub-intervals. During each sub-interval the geometry is considered constant. Before the next time interval is computed, the surface (and the mesh used for the flow computations) is updated to account for the ice accreted during the previous interval. Such a multi-step approach is used e.g. in [Gori et al. \(2015\)](#). A sensitivity study to physical and modelling parameters affecting airfoil icing using such an approach is shown

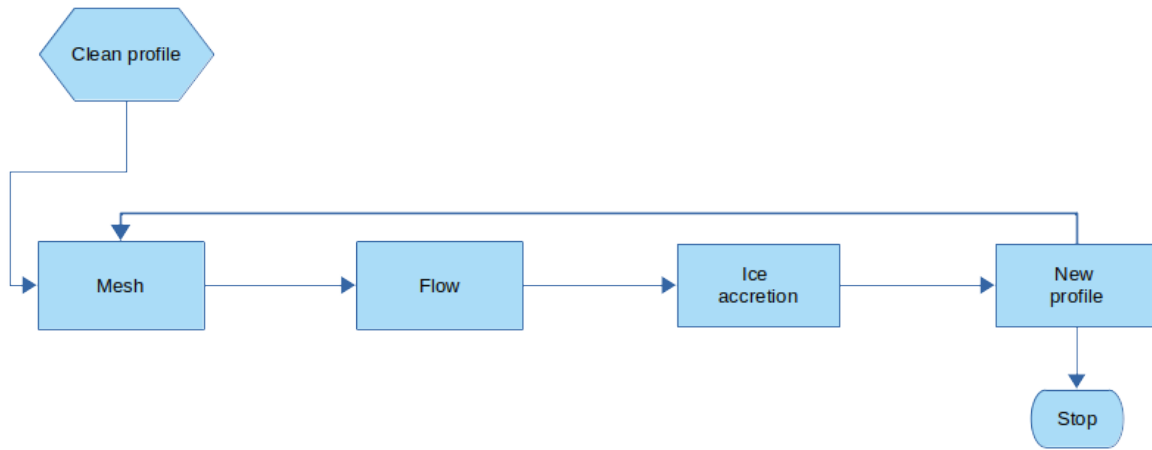


Fig. 1: Steps of the multi-staged approach

in Prince Raj et al. (2020).

Here, we use also such a multi-staged approach, the main steps being shown in Figure 1. The entire icing event will be computed in  $N_{st}$  steps. When choosing the number of iteration steps one has to consider that for severe ice accretion cases a too low number of steps would assume constant geometry of the airfoil for a too long physical time, thus having a negative impact on the accuracy of the predictions. At the other extreme, dividing the icing event into too many sub-intervals leads to very small changes in the airfoil shape, and therefore results in sub-optimal use of the computing resources. Consequently, the optimal number of steps is determined by the balance of the desired accuracy of the staged approach and the available computing time, and is case-dependent, being mainly a function of the severity of the ice accretion event.

The ice accretion simulations are performed using the open-source toolbox [OpenFOAM](#) in combination with an in-house tool to adjust the airfoil surface based on the amount of ice accreted.

The computations start with the clean airfoil as input. In order to reduce the time needed for the computations only two-dimensional domains are considered. The mesh is generated in two stages. First the `snappyHexMesh` utility (included in `OpenFOAM`) is used to generate an unstructured 3D mesh around the airfoil. Next, the 2D mesh is obtained by extruding one of the sides of the 3D mesh. For the purpose of improving the computational efficiency, the flow and ice accretion computations are separated. It is assumed that during a sub-stage the shape of the airfoil, and by this the flow, is not changing significantly. For this reason, the statistically stationary two-dimensional flow field is simulated first using the SST  $k-\omega$  RANS model (Menter (1994)). Thereafter, the ice accretion is determined by Lagrangian Particle Tracking (LPT) based on the steady flow field. The number of injected parcels and the injected droplets' diameter is determined to match the desired LWC. In the LPT computations only the particle drag force and the turbulent dispersion is accounted for. The turbulent dispersion is done with a stochastic model (a.k.a random walk).

Each parcel of Lagrangian particles that impacts the aerofoil surface is registered. Depending if rime- or glaze-ice conditions are computed, the droplet impacting the surface is considered to freeze immediately or is allowed to travel along the surface. The details of the glaze ice model are given in Section 3.

Once the amount and distribution of accreted ice is determined, the airfoil surface is updated using an in-house tool. Before updating the surface, two pre-processing stages are carried out.

First, the ice distribution is smoothed over the airfoil surface. This step is motivated by the fact, that even if the length of the LPT computations is long enough to achieve a statistically converged ice distribution, depending on the mesh resolution used to discretize the airfoil, there might be small cells with no ice accreted, leading to physically irregular shape of the ice accreted surface. This smoothing step is carried out by transferring the information of accreted ice in a mass-conservative manner from the cell centers to the mesh vortices and back. The effect of smoothing can be increased by increasing the number of smoothing loops. The second pre-processing of the accreted ice mass aims to increase performance. Since the time scale of the flow and the ice accretion differ substantially, with the icing time scale being much longer, one can increase the computational efficiency by scaling the amount of accreted ice everywhere by a factor  $f$ , leading to a shortening of the time covered by the LPT computations with the same factor,  $f$ . The scaling is limited by the fact that a too large scaling factor would lead to too short time intervals covered by the LPT computations and the results would not be repeatable due to the randomness involved in the Lagrangian approach. Thus there is a requirement of having statistically representative amount of ice (i.e. the distribution not changing by longer computations) accreted on the airfoil. Our previous investigations show that it is possible to decrease the time scale of ice accretion by a factor 1000, i.e., one second explicitly computed ice accretion can be scaled to predict accretion after 1000 s.

The new shape of the airfoil is determined by an iterative approach using an in-house tool. The tool reads in the surface mesh used in `OpenFOAM` to discretize the airfoil geometry and the amount of ice accreted on each mesh cell face. Based on the accreted ice mass and a user-provided density one can determine the added volume for each cell face and, by integrating it over all cells, the total ice volume to be added to the airfoil,  $dV_T$ . Based on the added volume, the face area and the face normal direction, one can compute an initial guess for the average displacement vector at each node of the surface mesh,  $\mathbf{dx}$ , as the average of the displacement vectors needed for the surrounding cells. Based on the average displacement, the first approximation of the ice-accreted mesh shape can be obtained by  $\mathbf{x}^1 = \mathbf{x}^0 + \omega \mathbf{dx}$ , where exponents 0 and 1 denote the old and new values, respectively,

and  $\omega$  is an under-relaxation factor (set to 0.8 in the present calculations). Based on the estimated positions of the surface nodes, the actually added ice volume,  $dV_A$ , can be determined. Since this volume usually differs from the target added volume, the positions of the surface mesh nodes are corrected iteratively using Equation 2, the stopping criterion being  $|(dV_T - dV_A^k)/dV_T| < 10^{-10}$ .

$$\mathbf{x}^{k+1} = \mathbf{x}^k + \omega \mathbf{dx} (dV_T - dV_A^k)/dV_T \quad (2)$$

Once the new airfoil shape is determined a new mesh is generated and the entire process is iterated until the total length of the icing event is covered.

### 3 Glaze ice model

#### 3.1 Goal

As mentioned earlier, in order to accurately model glaze ice conditions, one needs to use a multitude of interacting models to describe the impact of the droplets, the formation of the water film and the heat transfer between the air, the water film and the solid surfaces. The large number of required models renders the Computational Fluid Dynamics (CFD) computations heavy both directly, by increasing the computational time needed to evaluate the models, and indirectly due to slower convergence as a result of the large number of degrees of freedom. Furthermore, even if the individual models can be validated for certain conditions, when a large number of models are interacting the accuracy of the predictions may suffer.

Our goal was to develop a simpler and more efficient model to account for glaze conditions. The increased efficiency was planned to be achieved by reducing the number of physical phenomena explicitly accounted for which inherently leads to a reduced number of model parameters. As a drawback, the model is expected to be less general, requiring validation to adjust the model parameters.

#### 3.2 Model description

The glaze model is an extension of the rime-ice model initially implemented in an in-house solver (Szász and Fuchs (2012); Szász et al. (2016)) and later implemented in OpenFOAM as well. The main idea of the model is to not freeze instantaneously the parcels upon impact (as it is the case for rime ice), but let the droplets slide along the surface for a specified freezing time,  $ft$ . During this freezing period only the positions of the droplets are updated, the freezing conditions are not re-evaluated. Although this is a rather crude approximation, it is much more efficient than using e.g. a wall film model and heat transfer calculations.

Two options have been implemented for the time being: prescribed freezing time and a first order approximation.

##### 3.2.1 Prescribed freezing time

This simplified model, as the name suggests, requires that the user specifies the time delay,  $ft$ , until the droplets (modelling the wall film) freeze. Although very simplistic, this model adds very little computational effort, thus it is affordable to evaluate cases where rime-ice conditions can be evaluated. Although the accuracy is limited, one can easily carry out sensitivity studies and/or validation computations.

During validation computations, it was found that simply imposing a time delay is not sufficient to model glaze ice conditions, since the impacting droplets are deflecting from the surface. In reality the droplets more often attach to the wall due to surface tension effects. To account for this, an additional model parameter has been introduced,  $e$ , which can be used to adjust the elasticity of the impact, the normal component of the parcel velocity after impact being computed as  $\mathbf{u}_N = e \cdot \mathbf{u}_T$ ,  $\mathbf{u}_T$  being the tangential component. Thus, the normal component can be zeroed by setting  $e = 0$ . Nevertheless, cancelling the normal component entirely is not physical either because, upon impact, the droplets are located in regions of the boundary layer with very low relative velocity and even long time delays lead to very small displacements of the parcels along the surface. In reality the droplets and the wall film have a non-zero thickness and experience larger relative velocities.

##### 3.2.2 First order approximation

To avoid the need to directly impose the freezing time, a second possibility has been implemented. This approach is based on the heat transfer in a spherical droplet with uniform properties, initial temperature of  $T_i$  in a surrounding with the exterior temperature of  $T_e$ .

The governing equation in radial direction is:

$$\frac{1}{r^2} \frac{\partial}{\partial r} \left( r^2 \frac{\partial \theta}{\partial r} \right) = \frac{1}{\gamma} \frac{\partial \theta}{\partial t} \quad (3)$$

where  $\theta(r, t) = T - T_e$ . The solution of Eq.3 is of the form:

$$\theta(r, t) = \sum_{n=1}^{\infty} \frac{C_n}{r} \sin(\lambda_n r) \exp(-\gamma \lambda_n^2 t) \quad (4)$$

The coefficients are given by:

$$C_n = -\frac{T_i}{\lambda_n} (-1)^n \quad (5)$$

and

$$\lambda_n = \frac{n\pi}{R} \quad (6)$$

$R$  being the radius of the spherical droplet.

The idea of the first order approximation is that the  $C_n$  coefficients of the solution series in Equation 4 are decreasing with increasing  $n$ , in fact the first term is dominating in most cases. Thus, neglecting the terms for  $n > 1$ , from Equation 4 one can compute the time needed to freeze the droplet as:

$$ft = -\frac{1}{\lambda_1^2 \gamma} \ln \left( \frac{\theta_c r_c \lambda_1}{\theta_i \sin(\lambda_1 r_c)} \right) \quad (7)$$

$\theta_c = T_f - T_e$  is the critical temperature difference for freezing,  $r_c$  is the smallest radius we require to freeze (assuming that the front propagates from the exterior),  $r_c = 0.1R$  should be sufficient for most cases.

## 4 Results

Due to the inherent difficulties in carrying out ice accretion experiments, there is relatively little experimental data available in the literature reporting ice accretion results in well controlled conditions. We chose to apply the glaze ice model on three sets of data, Cases 1 and 3 from Hochart et al. (2008) and Run 308 from Wright and Rutkowski (1999).

### 4.1 Comparison to the data from Hochart et al.

#### 4.1.1 Case set up

In Hochart et al. (2008) ice accretion on a NACA 63415 airfoil is investigated in glaze and rime ice conditions. Cases 1 and 3 from Hochart et al. (2008) correspond to mild and severe glaze ice conditions, respectively. The details of the experimental conditions as well as the amount of accreted ice measured in the experiments are summarized in Table 1.

Tab. 1: Summary of the experimental cases Hochart et al. (2008)

Parameter	Case 1	Case 3
LWC [ $g/m^3$ ]	0.37	0.48
MVD [ $\mu m$ ]	27.6	27.6
$T_e$ [ $^{\circ}C$ ]	-1.4	-1.4
$u_{rel}$ [ $m/s$ ]	19.9	56.0
t [min]	14.8	24.8
$\alpha$ [ $^{\circ}$ ]	6	6
average accreted ice [g]	48	354
standard deviation [g]	0.25	4.5

The parameter choices and the resulting amount of accreted ice for the computed cases are shown in Table 2. The predictions for Case 1 used 12 loops and a scaling factor of  $f = 1000$  to predict the amount of accreted ice. Thus, each iteration in the loop computed the ice accretion for 0.074 s physical time and the airfoil surface was adjusted by assuming that the same trend is valid for 74 s. Since Case 3 involves more severe icing, the number of loops was increased to 25 (each iteration corresponds to 0.062 s), the scaling factor being the same as in Case 1.

A general observation is that the computations are consistently over-predicting the amount of accreted ice, the error being significantly larger for the case with severe icing condition. Furthermore, the predicted amount of accreted ice does not change significantly with changes in the model parameters.

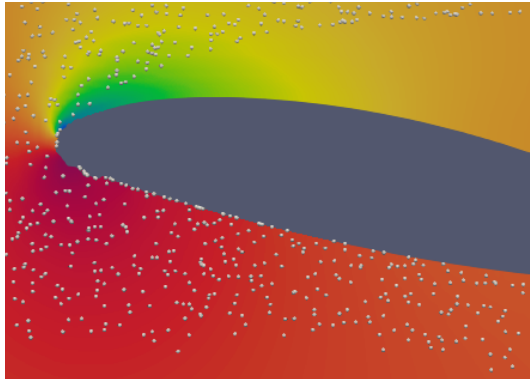
#### 4.1.2 Hochart Case 1

Figure 2 shows the isocolors of the average static pressure at the end of the ice accretion event (14.8 minutes) for Case 1. For visualization purposes, the instantaneous snapshots of the Lagrangian parcel field at the last calculated timestep is shown as well. Note, that the lagrangian field is uniformly down-sampled to improve visibility. Figure 2a shows the results when the model was set up to mimic rime ice conditions (by setting  $ft = 0$ ), whereas Figure 2b displays the results for  $ft = 0.1$  s and  $e = 0.5$ . One can observe the smoother ice shape in the leading edge region. Also the higher density of the parcels impacted on the surface stretches to a larger downstream distance in the glaze ice case compared to rime ice conditions.

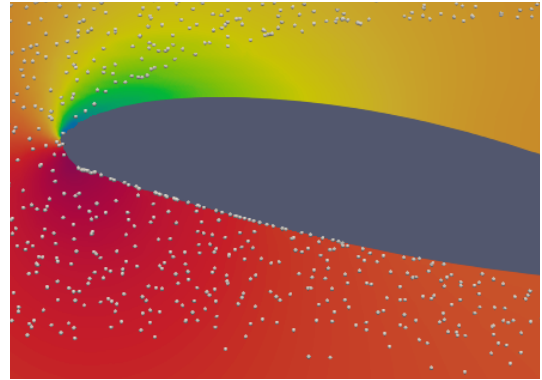
Tab. 2: Summary of the computed cases

Case	Case <sup>a</sup>	ft [s]	e [-]	Accre-ted ice mass [g]	Error [%]
C1T00	1	0.0	0.0	59.52	24.0
C1T01	1	0.1	0.0	59.40	23.7
C1T10	1	1.0	0.0	59.48	23.9
C1T01E05	1	0.1	0.5	59.32	23.6
C3T00	3	0.0	0.0	559.07	57.9
C3T01E05	3	0.1	0.5	563.05	59.1
C3T01E08	3	0.1	0.8	558.55	57.8

<sup>a</sup> Case number in [Hochart et al. \(2008\)](#)



(a) ft=0



(b) ft=0.1, e=0.5

Fig. 2: Illustration of the flow field for Case 1, (a) rime ice model and (b) glaze ice model

The influence of the imposed freezing time is illustrated in Figure 3. The figure shows the contour of the clean airfoil (black) together with ice accreted airfoils by setting the model parameter for the freezing time to 0 s (blue, modelling rime ice conditions), 0.1 s (red) and 1 s (green). As a comparison, the timescale based on the relative velocity and the chord length is 0.01 s. One can also compare these timescales to the timescale resulting from the first order approximation described in Section 3.2.2 which for the parameters reported in Table 1 is 0.006 s. The leading and trailing edge regions are enlarged for better visibility. One can observe that even allowing a relatively long freezing time, the shape of the ice does not change significantly. The reason is that the second model parameter,  $e$ , controlling the elasticity of the droplet collision with the surface was set to zero. As a consequence, the impacting droplet parcels were trapped in the low velocity region in the proximity of the wall, leading to very small displacements even for long freezing times.

The influence of the parameter controlling the elasticity of the impact is shown in Figure 4, where the clean airfoil (black) is compared to ice accreted airfoils with the same freezing time (0.1 s) but having  $e = 0$  (red, no rebound) and  $e = 0.5$  (orange, partially elastic collision). One can observe that adjusting the elasticity parameter leads only to minor changes in the accreted ice shape. The quantitative changes are also minor, the error decreases only with 0.1% (see table 2).

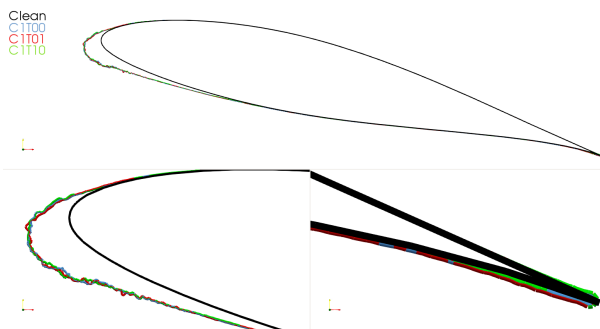


Fig. 3: Comparison of the clean and ice accreted airfoil contours for different values of the freezing time. Case 1. The lower images show zoomed-in details in the leading and trailing edge regions.

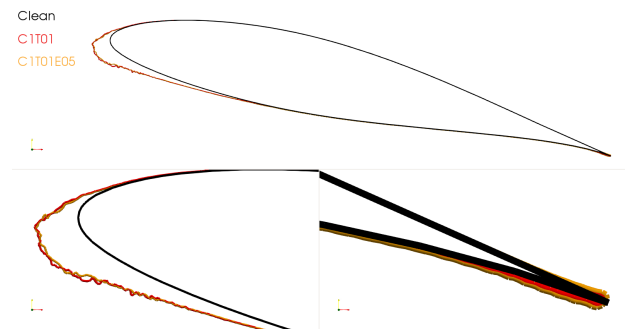


Fig. 4: Comparison of the clean and ice accreted airfoil contours for different values of the elasticity parameter. Case 1. The lower images show zoomed-in details in the leading and trailing edge regions.

### 4.1.3 Hochart Case 3

Case 3 corresponds to extreme icing conditions and was chosen in order to 'stress-test' the model, to emphasize limitations and clarify targets to be improved in the future.

Figure 5 shows the isocolors of static pressure and the droplet parcel field for Case 3 with three different settings of the model parameters. Figure 5a shows rime ice conditions ( $ft=0$ ), the other two subfigures illustrate glaze ice conditions with different settings of the elasticity parameter.

Unfortunately, all three computations resulted in significant over-prediction of the amount of accreted ice and in the formation of excessively large horn-like structures which are not likely to occur in reality. The closest resemblance to the experimentally observed shapes reported in Hochart et al. (2008) is found for  $ft=0.1$  s,  $e=0.5$  (Figure 5b): both the tendency to form a shape with two bumps on the suction side and to collect ice in the trailing edge region are captured qualitatively, however, the accreted ice does not have the smooth shape on the pressure side like in the experiments.

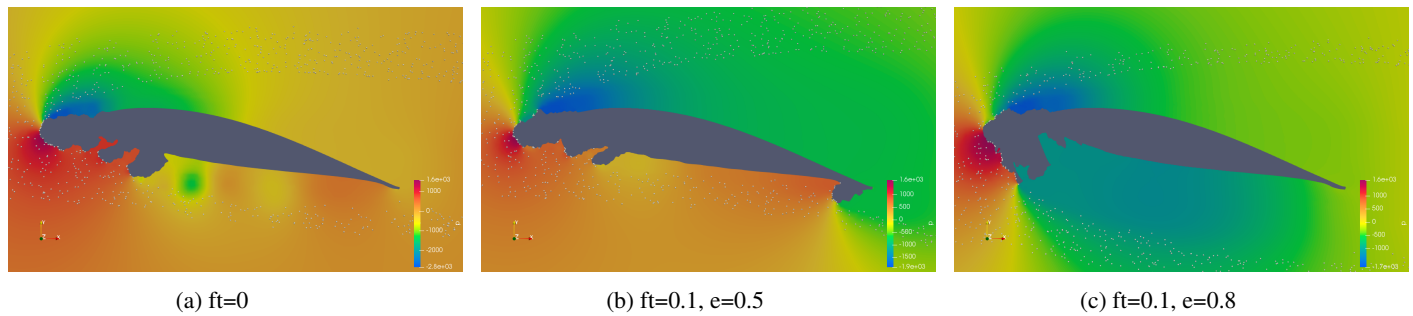


Fig. 5: Illustration of the flow field for Case 3 for three different parameter combinations

## 4.2 Comparison to the data from Wright et al.

### 4.2.1 Case set up

Among the multitude of cases reported in Wright and Rutkowski (1999) the case called Run 308 was chosen since it is a glaze ice case in relatively severe icing conditions. The main parameters describing the icing event are listed in Table 3.

Tab. 3: Summary of the experimental case Wright and Rutkowski (1999)

LWC [ $g/m^3$ ]	1.0
MVD [ $\mu m$ ]	20.0
$T_e$ [K]	262.04
$\underline{u}_{rel}$ [m/s]	102.8
t [min]	3.85
Airfoil	NACA 0012
$\alpha$ [ $^\circ$ ]	4

### 4.2.2 The influence of model parameters

Three parameters have been evaluated for this case.

The influence of smoothing of the accreted ice amount is visualized in Figure 6a. Three cases are shown with 1 (red), 10 (green) and 200 (blue) smoothing iterations. As it was expected, smoothing decreases the irregularity of the resulting ice surface. Furthermore, the amount of accreted ice changes as well, especially on the pressure side. The reason is that due to smoothing there are smaller irregularities in this region and fewer droplets are collected.

The influence of freezing time is shown in Figure 6b. The rime ice case ( $ft=0$ , blue) is compared to glaze model cases with  $ft=0.1$  s and  $ft=0.2$  s. The main impact of the freezing time in this set-up is the reduction of the amount of accreted ice. This is expected since the droplets do not freeze instantaneously. It was expected to see the limit of accreted ice further downstream for glaze conditions. Nevertheless, such effect cannot be observed, probably due to the shape of the accreted ice in the leading edge region. Finally, the influence of the elasticity parameter,  $e$ , is shown in Figure 6c. As it can be seen, with the decrease of  $e$  fewer droplets accrete on the surface, the  $e = 0.9$  case being very close to the results obtained in rime ice conditions.

## 4.3 Turbulence modeling effects

As it was shown in sections 4.1 and 4.2, for glaze ice conditions the suggested model always overpredicts the amount of accreted ice. One of the possible reasons for this overprediction is the choice of the turbulence model. In order to speed up the computations, RANS has been chosen to account for turbulent effects since for low angles of attacks and smooth airfoils it is expected to provide

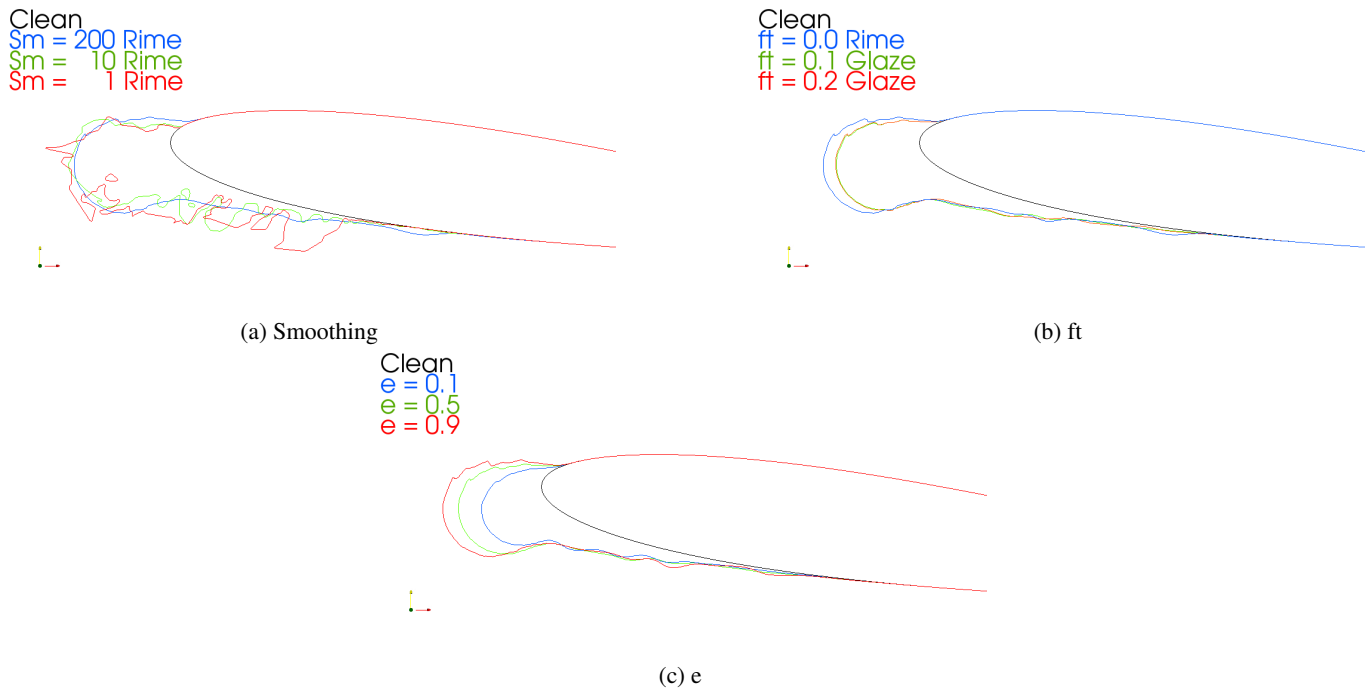


Fig. 6: Influence of the model parameters on the accreted ice shape.

results with good accuracy. However, for complex shapes, like the ones resulting from ice accretion, RANS-based models have difficulties to predict the average flowfield (see e.g. Figure 5a).

In order to assess the impact of turbulence modeling, a case based on Large Eddy Simulations (LES) has been set up as well. To compute an entire ice accretion event would have required significant computing resources; consequently, only one sub-cycle of an ice accretion event has been recomputed using LES.

At the beginning of the ice accretion phase, when the airfoil is still rather smooth, we expect no significant differences between LES and RANS computations. In contrary, at the end of the ice accretion event, the ice structures predicted by RANS are unphysically large and we expect that a comparison to LES simulations would not be relevant either. For these reasons, the target of the LES simulations was chosen to be a cycle approximately at halftime (12th out of 24) of the severe glaze ice accretion event 3 from Hochart et al. (2008). The ice accretion parameters are the same as the ones used in Case C3T01E05 (see Table 2), thus the LES results are to be compared to the RANS results obtained during the same sub-cycle of Case C3T01E05.

The computational domain size for the LES computations was the same as for the RANS case, except in the spanwise direction which was set to 0.08 m corresponding to 0.4 chord lengths. The boundary conditions in spanwise direction were set to symmetry. The airfoil geometry was the same as the one used to generate the mesh in the RANS case. In the LES case, an oct-tree based refined mesh was generated using the snappyHexMesh utility included in OpenFOAM. The smallest cell size in the RANS and LES computations is the same order of magnitude. Although this might not be sufficient for a proper LES simulation, it was deemed to be sufficient to indicate qualitatively the impact of changing the turbulence model. Of course, when higher accuracy is required, further refinement of the LES mesh is suggested. The resulting LES mesh included approximately 2 million cells which is an order of magnitude larger than the amount used in the RANS computations (see Table 4). As sub-grid scale model, the Wall-Adapting Local Eddy-Viscosity Model (WALE) has been used.

The ice accretion computations have been carried out similarly to the 2D computations presented in the previous sections. To speed up the computations, the flow field was initialized first with a steady RANS simulation. Contrarily to the 2D computations where the lagrangian field was transported by the frozen flow field predicted in the RANS simulation, in the LES case both the flow and the lagrangian fields were developing simultaneously. The computations have been carried out in two stages, first the flow was let to develop by the LES solver from the steady flow field. Next, the eventually accreted ice during the developing phase is removed and the simultaneous flow and ice accretion simulation is carried out for the same time as in the 2D case.

The accreted amount of ice is visualized in Figure 7 for the RANS (first row) and LES (second row) cases. Since the magnitudes are different in the 2D and 3D cases, the accreted ice mass is normalized with its maximum value for each specific case. Comparing the RANS and LES cases no significant differences can be seen in the accreted ice distribution, neither on the pressure or suction sides. To emphasize the differences, the last row of Figure 7 shows the airfoil shapes after the morphing stage, red color is used for RANS and green for the profile obtained with LES. Note that the RANS airfoil has a finite span but the computations have been carried out in a 2D manner.

One can observe that on the suction side the two profiles are practically collocated, there is only a small region at the leading edge where the red color indicates that more ice is predicted in the RANS case, and a small region approximately at half chord length which is purely green, indicating more ice in the LES case.

On the pressure side, close to the leading edge, the two profiles are again practically collocated, indicating similar amount of accreted ice. Further downstream, however, there is a long region where the dominating green color indicates more accreted ice in the LES case. Contrarily, at the trailing edge the clear red color shows that RANS predicted more accreted ice.

Examining the final predicted ice shape for the considered case (Fig. 5b) one can conclude that the qualitative differences indicated in Figures 7e and 7f act against the formation of the large unphysical structures developed in the RANS computations, especially the one formed at the trailing edge.

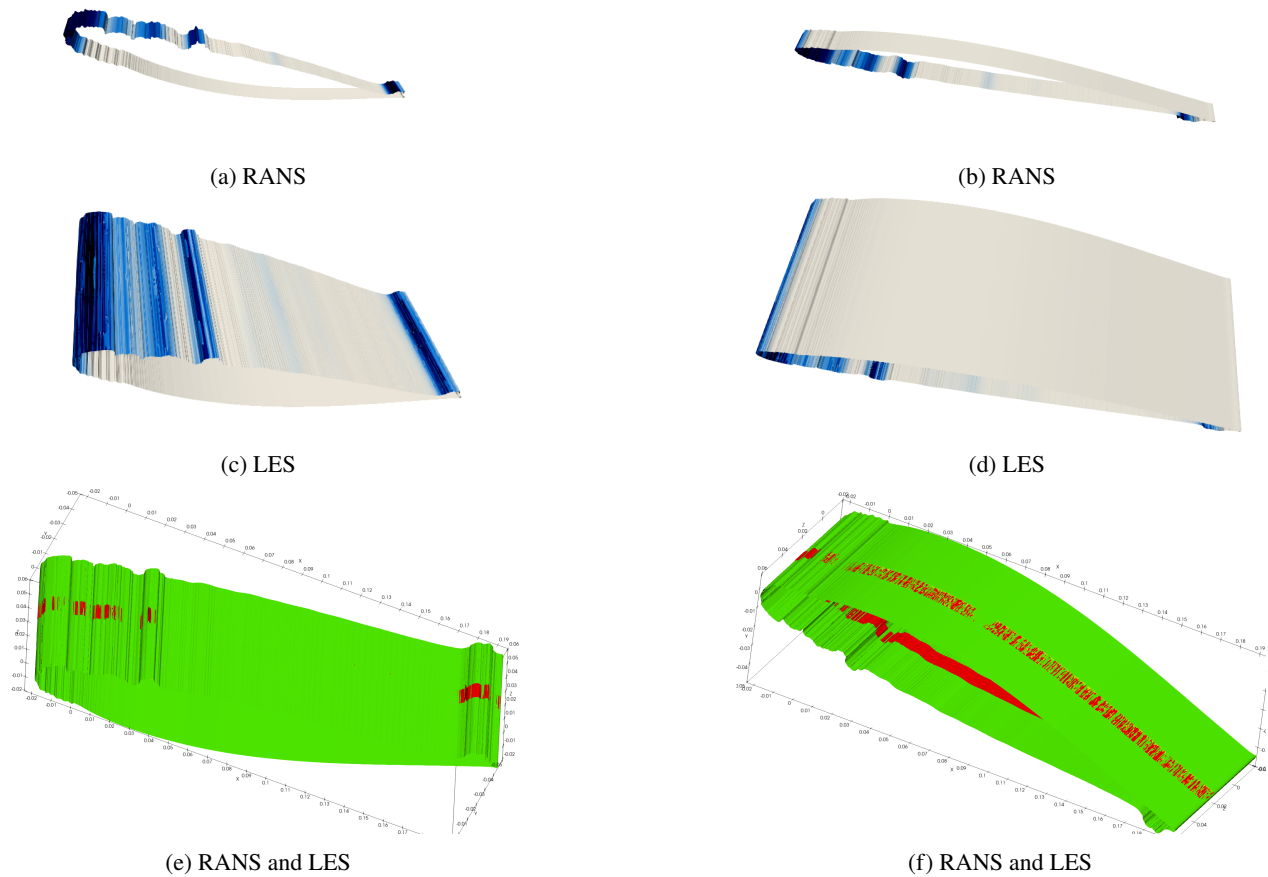


Fig. 7: Accreted ice amount for RANS (first row) and LES (second row). Overimposed airfoil shapes for RANS (red) and LES (green) (third row). Pressure side (left) and suction side(right)

For a quantitative analysis, the amount of predicted ice is shown in Table 4. As one can observe, an approximately 5% reduction of the accreted ice is seen in the LES case. Although this reduction is relatively small compared to the total error in predicting the ice mass, one needs to remember that this simulation was reproducing only one of the ice accretion sub-intervals, the entire ice accretion event has been previously simulated with RANS using 24 cycles. As a consequence, it is expected, that simulating the entire ice accretion event using LES would reduce the error with definitely more than 5%.

Besides the accreted ice mass, Table 4 shows also the number of cells used for the simulations and the number of CPU hours needed to carry out the main accretion simulation (i.e. not including the part to initialize the flow field with RANS and to develop the lagrangian and LES fields). The reported CPU hours were measured on the same hardware (16 cores of an AMD Ryzen Threadripper 2990WX processor). It is obvious, that even for the LES resolution used herein, the increase of the required computing resources is huge. Consequently, LES simulations do offer the possibility to increase the accuracy, but at a significant price and are not really feasible in situations where a large number of ice accretion events have to be computed.

Tab. 4: Comparison of the RANS and LES computations

Case	$N_{cells}$	CPUh	Accreted ice [g/m]
RANS	221051	0.72	0.049985
LES	2071276	1920.3	0.0473246
Difference [%]	837	268256	-5.32

## 5 Summary

This work has been a first attempt to implement a fast ice accretion model applicable for glaze ice conditions. Considering the fact that the amount of physical models is significantly reduced we deem that the accuracy of the model is reasonable for mild icing conditions. For severe icing conditions; however, the error in the predicted ice mass increases significantly and unexpected ice shapes are formed, thus further model improvements are needed.

We investigated one of the possible error sources, namely the use of 2D RANS computations to predict the flow fields. A comparison with an equivalent LES computation revealed that indeed, using more advanced modeling approaches will improve the

prediction of the amount of accreted ice.

Both the overprediction of the amount of ice and the shape of the ice structures indicate that one significant deficiency of the model is that it does not account for ice loss due to shedding. In reality, ice horns might break due to the aerodynamic forces acting on them. Thus, an important improvement of the model would be to account for ice loss, that feature being important both for rime and glaze ice conditions. We expect that by allowing ice loss both the amount of accreted ice and its shape would be closer to the experimentally observed ones. By removing the protruding ice horns, fewer droplet parcels would be captured in the leading edge region and more parcels are expected to deposit further downstream on the pressure side, as it was observed in the experiments. The model parameters have been adjusted in an ad-hoc manner so far. However, when more experimental data will be available, we expect that the model parameters could be more systematically validated and correlations between icing conditions and the model parameters can be found.

## Acknowledgements

Financial support for this work was provided by the Swedish Energy Agency, project no. 47053-1. The computational resources were provided by the Swedish National Infrastructure for Computing (SNIC), partially funded by the Swedish Research Council through grant agreement no. 2018-05973 and by LUNARC.

## References

- C. Antonini, M. Innocenti, T. Horn, M. Marengo, and A. Amirfazli. Understanding the effect of superhydrophobic coatings on energy reduction in anti-icing systems. *Cold Regions Science and Technology*, 67(1-2):58–67, jun 2011. ISSN 0165232X. doi: [10.1016/j.coldregions.2011.02.006](https://doi.org/10.1016/j.coldregions.2011.02.006). URL <http://dx.doi.org/10.1016/j.coldregions.2011.02.006https://linkinghub.elsevier.com/retrieve/pii/S0165232X11000401>.
- Daniel Badman and Ylva Tengblad. Roadmap 2040Wind power: Combating climate change and improving competitiveness. Technical report, Swedish Wind Energy Association, 2021. URL <https://swedishwindenergy.com/press-releases/revised-road-map-2040-wind-power-combating-climate-change-and-improving-competitiveness>.
- Andy Broeren, Christopher LaMarre, Michael Bragg, and Sam Lee. Characteristics of SLD Ice Accretions on Airfoils and Their Aerodynamic Effects. In *43rd AIAA Aerospace Sciences Meeting and Exhibit*, pages 3027–3050, Reston, Virginia, jan 2005. American Institute of Aeronautics and Astronautics. ISBN 978-1-62410-064-2. doi: [10.2514/6.2005-75](https://doi.org/10.2514/6.2005-75). URL <https://arc.aiaa.org/doi/10.2514/6.2005-75>.
- G. Gori, M. Zocca, M. Garabelli, A. Guardone, and G. Quaranta. PoliMIce: A simulation framework for three-dimensional ice accretion. *Applied Mathematics and Computation*, 267:96–107, sep 2015. ISSN 00963003. doi: [10.1016/j.amc.2015.05.081](https://doi.org/10.1016/j.amc.2015.05.081). URL <http://dx.doi.org/10.1016/j.amc.2015.05.081https://linkinghub.elsevier.com/retrieve/pii/S0096300315007055>.
- B.G. Gulick. Effect of simulated iced formation on the aerodynamic characteristics of an airfoil. Technical Report R.N. NACA-Wr.L-292, NACA, 1938.
- Clement Hochart, Guy Fortin, Jean Perron, and Adrian Ilinca. Wind turbine performance under icing conditions. *Wind Energy*, 11(4):319–333, July 2008. ISSN 10954244. doi: [10.1002/we.258](https://doi.org/10.1002/we.258). URL <http://doi.wiley.com/10.1002/we.258>.
- Matthew C. Homola, Muhammad S. Virk, Tomas Wallenius, Per J. Nicklasson, and Per A. Sundsbø. Effect of atmospheric temperature and droplet size variation on ice accretion of wind turbine blades. *Journal of Wind Engineering and Industrial Aerodynamics*, 98(12):724–729, August 2010. ISSN 01676105. doi: [10.1016/j.jweia.2010.06.007](https://doi.org/10.1016/j.jweia.2010.06.007). URL <http://linkinghub.elsevier.com/retrieve/pii/S0167610510000693>.
- Jia Yi Jin and Muhammad Shakeel Virk. Study of ice accretion and icing effects on aerodynamic characteristics of DU96 wind turbine blade profile. *Cold Regions Science and Technology*, 160(September 2018):119–127, apr 2019. ISSN 0165232X. doi: [10.1016/j.coldregions.2019.01.011](https://doi.org/10.1016/j.coldregions.2019.01.011). URL <https://linkinghub.elsevier.com/retrieve/pii/S0165232X18304476>.
- R. Jones and D. Williams. The effect of surface roughness of the characteristics of the airfoils NACA 0012 and RAF 34. Technical Report Report No.1708, British ARC, 1936.
- D.M. Kintea, I.V. Roisman, and C. Tropea. Transport processes in a wet granular ice layer: Model for ice accretion and shedding. *International Journal of Heat and Mass Transfer*, 97:461–472, jun 2016. ISSN 00179310. doi: [10.1016/j.ijheatmasstransfer.2016.01.076](https://doi.org/10.1016/j.ijheatmasstransfer.2016.01.076). URL <http://dx.doi.org/10.1016/j.ijheatmasstransfer.2016.01.076https://linkinghub.elsevier.com/retrieve/pii/S0017931015312758>.
- Timo Laakso, Ian Baring-Gould, Michael Durstewitz, Robert Horbaty, Antoine Lacroix, Esa Peltola, Göran Ronsten, Lars Tallhaug, and Tomas Wallenius. State-of-the-art of wind energy in cold climates, 2010. ISSN 1459-7683. URL <http://www.vtt.fi/publications/index.jsp>.
- Eric Laurendeau, Simon Bourgault-Cote, Isik A. Ozcer, Richard Hann, Emmanuel Radenac, and Alberto Pueyo. Summary from the 1st AIAA Ice Prediction Workshop. In *AIAA AVIATION 2022 Forum*, pages 1–27, Reston, Virginia, jun 2022. American Institute of Aeronautics and Astronautics. ISBN 978-1-62410-635-4. doi: [10.2514/6.2022-3398](https://doi.org/10.2514/6.2022-3398). URL <https://arc.aiaa.org/doi/10.2514/6.2022-3398>.
- L. Makkonen. Models for the growth of rime, glaze, icicles and wet snow on structures. *Philosophical Transactions of the Royal Society A: Mathematical, Physical and Engineering Sciences*, 358(1776):2913–2939, November 2000. ISSN 1364-503X. doi: [10.1098/rsta.2000.0690](https://doi.org/10.1098/rsta.2000.0690). URL <http://rsta.royalsocietypublishing.org/cgi/doi/10.1098/rsta.2000.0690>.
- Lasse Makkonen. Heat transfer and icing of a rough cylinder. *Cold Regions Science and Technology*, 10:105–116, 1985.

- F.R. Menter. Two-equation eddy-viscosity turbulence models for engineering applications. *AIAA Journal*, 32:1598–1605, 1994.
- Bernard R. Messinger. Equilibrium temperature of an unheated icing surface as a function of air speed. *Journal of the Aeronautical Sciences*, pages 29–42, 1953. doi: [10.2514/8.2520](https://doi.org/10.2514/8.2520).
- Tim G. Myers. Extension to the messinger model for aircraft icing. *AIAA Journal*, 39(2), 2001. doi: [10.2514/2.1312](https://doi.org/10.2514/2.1312).
- OpenFOAM. OpenFOAM, <https://www.openfoam.org>. URL <https://www.openfoam.org>. Checked 2020.04.03.
- L. Prince Raj, K. Yee, and R.S. Myong. Sensitivity of ice accretion and aerodynamic performance degradation to critical physical and modeling parameters affecting airfoil icing. *Aerospace Science and Technology*, 98:105659, mar 2020. ISSN 12709638. doi: [10.1016/j.ast.2019.105659](https://doi.org/10.1016/j.ast.2019.105659). URL <https://doi.org/10.1016/j.ast.2019.105659https://linkinghub.elsevier.com/retrieve/pii/S127096381931805X>.
- P. Rauschenberger, A. Criscione, K. Eisenschmidt, D. Kintea, S. Jakirlić, Ž Tuković, I.V. Roisman, B. Weigand, and C. Tropea. Comparative assessment of Volume-of-Fluid and Level-Set methods by relevance to dendritic ice growth in supercooled water. *Computers & Fluids*, 79:44–52, jun 2013. ISSN 00457930. doi: [10.1016/j.compfluid.2013.03.010](https://doi.org/10.1016/j.compfluid.2013.03.010). URL <https://linkinghub.elsevier.com/retrieve/pii/S0045793013000996>.
- I. V. Roisman and C. Tropea. Impact of a drop onto a wetted wall: description of crown formation and propagation. *Journal of Fluid Mechanics*, 472:373–397, dec 2002. ISSN 0022-1120. doi: [10.1017/S0022112002002434](https://doi.org/10.1017/S0022112002002434). URL <https://www.cambridge.org/core/product/identifier/S0022112002002434/type/journal-article>.
- Markus Schreimb, Ilia V. Roisman, and Cameron Tropea. Normal impact of supercooled water drops onto a smooth ice surface: experiments and modelling. *Journal of Fluid Mechanics*, 835:1087–1107, jan 2018. ISSN 0022-1120. doi: [10.1017/jfm.2017.797](https://doi.org/10.1017/jfm.2017.797). URL <https://www.cambridge.org/core/product/identifier/S0022112017007972/type/journal-article>.
- Chankyu Son and Taeseong Kim. Development of an icing simulation code for rotating wind turbines. *Journal of Wind Engineering and Industrial Aerodynamics*, 203(June):104239, aug 2020. ISSN 01676105. doi: [10.1016/j.jweia.2020.104239](https://doi.org/10.1016/j.jweia.2020.104239). URL <https://doi.org/10.1016/j.jweia.2020.104239https://linkinghub.elsevier.com/retrieve/pii/S0167610520301495>.
- D. B. Stoyanov and J. D. Nixon. Alternative operational strategies for wind turbines in cold climates. *Renewable Energy*, 145: 2694–2706, January 2020. doi: [10.1016/j.renene.2019.08.023](https://doi.org/10.1016/j.renene.2019.08.023).
- Robert-Zoltan Szasz, Matilda Ronnfors, and Johan Revstedt. Influence of ice accretion on the noise generated by an airfoil section. *International Journal of Heat and Fluid Flow*, 62:83–92, 2016. ISSN 0142-727X. doi: [10.1016/j.ijheatfluidflow.2016.06.006](https://doi.org/10.1016/j.ijheatfluidflow.2016.06.006). URL <http://dx.doi.org/10.1016/j.ijheatfluidflow.2016.06.006>.
- R.Z. Szasz and L. Fuchs. Numerical modeling of ice accretion on a wing section. In J. Vad, editor, *Proceedings of the Conference on Modelling Fluid Flow*, pages 292–298, 2012.
- Mario Vargas, Jen-Ching Tsao, and Alric Rothmayer. Review of Role of Icing Feathers in Ice Accretion Formation. In *SAE Technical Papers*, volume 116, pages 589–601, sep 2007. doi: [10.4271/2007-01-3294](https://doi.org/10.4271/2007-01-3294). URL <https://www.jstor.org/stable/44719493https://www.sae.org/content/2007-01-3294/>.
- William Wright. User 's Manual for LEWICE Version 3 . 2. Technical Report NASA/CR–2008-214255, NASA, 2008.
- William B Wright and Adam Rutkowski. Validation Results for LEWICE 2.0. Technical report, Lewis Research Center, jan 1999.
- William B. Wright, Mark G. Potapczuk, and Laurie H. Levinson. Comparison of LEWICE and GlennICE in the SLD regime. *46th AIAA Aerospace Sciences Meeting and Exhibit*, (January 2008), 2008. doi: [10.2514/6.2008-439](https://doi.org/10.2514/6.2008-439).